

# Entropy evaluation sheds light on ecosystem complexity

Mattia Miotto\* and Lorenzo Monacelli†

*Department of Physics, University “Sapienza”, Piazzale Aldo Moro 5, 00185, Rome, Italy*

(Dated: June 15, 2021)

Preserving biodiversity and ecosystem stability is a challenge that can be pursued through modern statistical mechanics modeling. Here we introduce a variational maximum entropy-based algorithm to evaluate the entropy in a minimal ecosystem on a lattice in which two species struggle for survival. The method quantitatively reproduces the scale-free law of the prey shoals size, where the simpler mean-field approach fails: the direct near neighbor correlations are found to be the fundamental ingredient describing the system self-organized behavior. Furthermore, entropy allows the measurement of structural ordering, that is found to be a key ingredient in characterizing two different coexistence behaviors, one where predators form localized patches in a sea of preys and another where species display more complex patterns. The general nature of the introduced method paves the way for its application in many other systems of interest.

## I. INTRODUCTION

The general formulation of statistical mechanics and information theory opened the way of physics to complex systems. The entropy definition is the basis of both theories. Although the concept of entropy first appeared in thermodynamics, it has been adapted to other fields of study, including economics, biophysics, and ecology.

In this work, we focus our attention on an ecological system and its entropy, which we show to be pivotal in understanding how the phenotype, the characteristics of an organism resulting from the interaction between its genotype and the environment [1, 2], discriminates and provides information about survival and extinction of species. This is a very important effort that must be pursued in order to prevent ecological disasters.

In a very general way, entropy is a property of the distribution function out of which the states of the system have been drawn. It is the capacity of the data to provide or convey information [3]. Consequently, knowing the entropy allows us to set limits on the information we can extract from observations and to the predictability of the system. It has been widely used to study information transport in neural networks [4, 5] and in flocks of birds [6–8], complexity and hierarchy in written languages [9] and risk analysis in financial markets [10, 11]. In particular, predictability plays a very important role in economics where the awareness of markets entropy allows us to maximize the investment profits [10]. Recently, entropy has been exploited in inference problems, with great results in biological phenomena, such as bacterial growth [12, 13], evolution [14] and protein folding [15].

Here, we show how entropy is crucial also in the context of ecological systems. Ecosystems can be defined as a community of living organisms in conjunction with the environment [16, 17], where the latter affects the organisms without being in turn influenced by them [18]. On

the other hand, all living beings within the ecosystem are interdependent, in fact, variations in the size of one population influence all others. This is particularly clear for prey and predator dynamics. In fact, if the number of preys in an ecosystem grows, predators will respond to the supply of available food by increasing their number. The growth of predator number will reduce preys until the system can no longer sustain the predator population. The process has either to attain a steady state or to end in species extinction. In order to avoid extinction, both preys and predators need to optimize their phenotypes: predators must, for example, adapt for improving efficiency in hunting to catch enough food to ensure survival. Prey species, on the other hand, must be proficient in escaping their predators and reproduction; if enough of them are to survive for the species to endure [19–21]. Disturbances, which are perturbations that move the system away from its steady state [22], may affect species phenotypes. Such disturbances can originate from changing of environmental variables such as temperature and precipitation or in modifications of the populations, like the appearance/disappearance of a species. Besides the theoretical challenge of understanding the behavior of that kind of complex systems, worthy of notice is also the practical importance of predicting the response to perturbations, particularly the ones produced by humans. Relevant cases are the fight against parasites in agriculture [23] and the perturbations in sea populations due to fishing activities [24]. From the groundbreaking works of Lotka [25] and Volterra [26] ecosystem modeling has been addressed in various ways, from sets of differential equations [27–29] to simulations on lattice [30–32].

Taking inspiration from the work of Dewdney [33] we modeled the simplest nontrivial ecosystem in which two species struggle for survival. Sharks (predators) and fishes (preys) occupy the nodes of the toroidal 2D lattice; they can move, reproduce and hunt. The rules of the model resemble the ones described by Mobilia et al. [34] and are introduced in Sec. III A. This system has been extensively studied and several critical behaviors have been observed [35, 36].

Measuring the entropy of this kind of complex system

---

\*Electronic address: [mattia.miotto@roma1.infn.it](mailto:mattia.miotto@roma1.infn.it)

†Electronic address: [lorenzo.monacelli@roma1.infn.it](mailto:lorenzo.monacelli@roma1.infn.it)

without any explicit expression for a *prior* probability distribution is very challenging [37]. In fact, the Shannon definition of entropy relies on the system probability distribution  $P$ , which depends on all the degrees of freedom of the system [38]. The entropy measurement requires a fine sampling of this function, becoming not affordable even for small lattices.

The Maximum Entropy (MaxEnt) technique has been developed in order to obtain an approximation for the probability distribution. Given a set of observables  $x_i$  that partially describes the inquired system, MaxEnt algorithm allows finding the less structured probability distribution that reproduces the chosen set of the real system observables. This technique was firstly introduced by Jaynes [39] in 1957, but it reached an outstanding interest only recently thanks to the availability of a huge amount of experimental and numerical data. MaxEnt has been successfully applied to countless problems, both in equilibrium and out-of-equilibrium systems [40]; among them, the prediction of protein amino acid contacts [15, 41] and the analysis of neural networks [42] are of particular interest. However, even if MaxEnt enables one to extract an analytic expression for the probability distribution, computing the associated entropy is still a major issue [7].

In sec. II A we outline how it is possible to obtain the exact entropy of the MaxEnt probability distribution taking advantage of all the data generated during the convergence of the algorithm, without any further time-consuming computation. Furthermore, in sec. II B, we introduce a *least* entropy principle that justifies the use of the MaxEnt distribution as a truncation of a series that converges toward the real entropy of the system. Availing the variational principle, the approximation on the resulting entropy is of second order. While the method is formally derived for dealing with equilibrium systems, in sec. III we apply it to the study of an ecosystem. In sec. III D we examine the insights the entropy provides and discuss its limitations in the case of a non-equilibrium steady-state system, like the one we treat. Although we apply this method only to the introduced ecosystem, it is very general: it can be used whenever it is possible to define a probability distribution on a site model.

### A. Maximum Entropy

The MaxEnt framework we are going to discuss can deal with any stochastic process defined on a graph composed of  $M$  nodes. Each node is in one out of  $q$  possible states. If we indicate with  $P$  the probability that the system is in a given configuration the entropy is defined accordingly to Boltzmann-Shannon as:

$$S[P] = -\langle \ln P \rangle_P, \quad (1)$$

where  $\langle \cdot \rangle_P$  indicates the average over the  $P$  probability distribution.

The standard MaxEnt algorithm consists in maximizing  $S[P]$  with respect to  $P$  in presence of a set of  $N$  constraints. The restraints are the set of observables  $\{x_i\}_{i=1}^N$  that best describes the system; in other words, some degrees of freedom are fixed and the entropy is maximized among the remaining ones in order to have the broadest possible probability function. Each observable  $x_i$  is a generic function that associates any possible configuration of the system to a real number. Note that the index  $i$  identifies the observable in the set of constraints, not the specific site on the graph, as the  $x_i$  observable can be a function of more than one node, e.g. the average dimension of clusters of nodes in the same state.

Defining the auxiliary Lagrange functional  $\Phi$  as:

$$\Phi[P, \lambda_1, \dots, \lambda_n] = -S[P] + \sum_{i=1}^N \lambda_i \langle x_i \rangle_P, \quad (2)$$

the correct constrained maximum entropy distribution  $P^*$  is found solving the set of equations:

$$\frac{\delta \Phi}{\delta P^*} = 0 \quad (3a)$$

$$\langle x_i \rangle_{P^*} = \bar{x}_i \quad \forall i = 1, \dots, N \quad (3b)$$

where  $\bar{x}_i$  is the measured expected value of  $x_i$ . Eq. (3) is very hard to solve, even numerically, since  $P$  depends still on  $q^M$  variables.  $P$  can be used to define an auxiliary effective Hamiltonian, according to the Boltzmann definition:

$$P(\vec{\sigma}) = \frac{e^{-H(\vec{\sigma})}}{Z},$$

where  $\vec{\sigma}$  represents the configuration and  $Z$  the partition function that normalizes  $P$ .

Eq. (3a) is solved by the Hamiltonian [39]:

$$H = \sum_{i=1}^N \lambda_i x_i, \quad (4)$$

where  $\lambda_i$  are fixed so that the expectation values of  $x_i$  respect the bounds over the real observables.

The values of  $\lambda_i$  can be obtained analytically only in very few cases. The simplest one is the mean-field solution, where only one-body observables are constrained, e.g. the numbers of nodes in each state. In the latter case the number of observables is equal to the number of states  $q$  and the Lagrange multipliers that satisfy the imposed constraints are:

$$\lambda_i = -\ln \left( \frac{\bar{x}_i}{M} \right). \quad (5)$$

The passages to prove Eq. (5) are sketched in appendix A. In this case, the entropy per node is:

$$S' = -\sum_{i=1}^q \left( \frac{\bar{x}_i}{M} \right) \ln \left( \frac{\bar{x}_i}{M} \right), \quad (6a)$$

$$S = MS'. \quad (6b)$$

This entropy evaluation corresponds to the standard one obtained by the Shannon-Fano algorithm [43, 44]. This is a ‘Hartree-Fock’ theory of the complex system, where the entropy is maximized using topology-independent Hamiltonians only. This framework paves the way to a more precise entropy computation.

## II. ENTROPY ALGORITHM

The general solution of Eq. (3) has been matter of discussion [42, 45–48]. On the way of Bialek and Ranganathan [48], we introduce an auxiliary function  $\tilde{\chi}^2$  whose global minimum coincides with the solution.

$$\tilde{\chi}^2 = \sum_{i=1}^N W_i (\langle x_i \rangle_H - \bar{x}_i)^2, \quad (7)$$

where  $\langle x_i \rangle_H$  is the average of the  $x_i$  observable computed using the trial Hamiltonian  $H$  while  $\bar{x}_i$  is the average over the real observable evaluated by the data.  $W_i$  are coefficients that do not affect the minimum of the  $\chi^2$ , however, if wisely chosen, may accelerate the convergence process. The  $\tilde{\chi}^2$  function defined in Eq. (7), in the minimum, is a random distributed Pearson variable only if all the observables are independent of each other and the  $W_i$  correspond to the inverses of the variances. This is not true in most MaxEnt applications, e.g. in the mean field case where the sum of the  $x_i$  is fixed to  $M$ .

We propose the introduction of a corrected  $\chi^2$  that takes into account linear correlations.

$$\chi^2 = \sum_{\substack{i=1 \\ j=1}}^N (\bar{x}_i - \langle x_i \rangle_H) (\Sigma^{-1})_{ij} (\bar{x}_j - \langle x_j \rangle_H), \quad (8)$$

where  $\Sigma$  is the covariance matrix between the  $N$  chosen observables. It must be stressed that Eq. (8) is still not a true  $\chi^2$  variable since we corrected only linear correlations. Moreover, eigenvectors of  $\Sigma$  will be uncorrelated, but not necessarily independent. However, the linear approximation for correlations between observables has a long history in statistical analysis [49, 50] and usually leads to very good results.

Eq. (8) is well defined only if  $\Sigma$  can be inverted. Diagonalizing the covariance matrix  $\Sigma$ , we can restrict the minimization only in the subspace spanned by its eigenvectors whose eigenvalues are greater than zero. Using these eigenvectors  $y_i$  as a basis, the Pearson  $\chi^2$  can be redefined as:

$$\chi^2 = \sum_{i=1}^{N'} \frac{(\bar{y}_i - \langle y_i \rangle_H)^2}{\tilde{\sigma}_i^2}, \quad (9a)$$

$$N' = N - \dim \ker \Sigma, \quad (9b)$$

$$y_i = \sum_{j=1}^N S_{ij} x_j, \quad (9c)$$

where  $\tilde{\sigma}_i^2$  is the  $i$ -th eigenvalue of the  $\Sigma$  matrix and  $S$  is a  $N' \times N$  matrix that diagonalizes  $\Sigma$ . The  $\dim \ker \Sigma$  indicates the dimension of the  $\Sigma$  kernel.

The gradient of Eq. (8) can be computed as follows:

$$\frac{\partial \chi^2}{\partial \lambda_k} = -2 \sum_{i=1}^{N'} \frac{(\bar{y}_i - \langle y_i \rangle_H)}{\tilde{\sigma}_i^2} \frac{\partial \langle y_i \rangle_H}{\partial \lambda_k}, \quad (10a)$$

$$\frac{\partial \langle y_i \rangle_H}{\partial \lambda_k} = \sum_{j=1}^N S_{ij} \frac{\partial \langle x_j \rangle_H}{\partial \lambda_k}, \quad (10b)$$

$$\frac{\partial \langle x_j \rangle_H}{\partial \lambda_k} = -\sigma_{jk}^{MC}. \quad (10c)$$

where  $\sigma_{jk}^{MC}$  is the covariance matrix between observables  $x_j$  and  $x_k$  for the current Hamiltonian:

$$\sigma_{jk}^{MC} = \langle x_j x_k \rangle_H - \langle x_j \rangle_H \langle x_k \rangle_H. \quad (11)$$

The final expression of the gradient is:

$$\frac{\partial \chi^2}{\partial \lambda_k} = 2 \sum_{i=1}^{N'} \frac{(\bar{y}_i - \langle y_i \rangle_H)}{\tilde{\sigma}_i^2} \sum_{j=1}^N S_{ij} \sigma_{jk}^{MC}, \quad (12)$$

or, equivalently, in a compact form:

$$\vec{\nabla} \chi^2 = 2S^\dagger \sigma'_{MC} \left( \frac{\vec{\Delta} y}{\sigma^2} \right), \quad (13)$$

where  $\sigma'_{MC}$  is the Monte Carlo covariance matrix in the non singular subspace and  $\vec{\Delta} y / \sigma^2$  is the vector:

$$\left( \frac{\vec{\Delta} y}{\sigma^2} \right)_i = \frac{\bar{y}_i - \langle y_i \rangle_H}{\tilde{\sigma}_i^2}. \quad (14)$$

The minimization of Eq. (8) can be initialized by the mean-field solution (5), choosing zero for each  $\lambda_i$  associated with a non topology-independent observable. Eq. (12) ensures that any standard gradient-based minimization algorithm can be used.

Moreover, in order to fasten the convergence[51], it is possible to derive the expression of the Hessian matrix in the minimum and utilize it as a precondition on the minimization:

$$D_{hk} = \left. \frac{\partial^2 \chi^2}{\partial \lambda_k \partial \lambda_h} \right|_{\vec{\nabla} \chi^2 = 0}, \quad (15)$$

$$D_{hk} = 2 \sum_{i=1}^{N'} \frac{1}{\tilde{\sigma}_i^2} \sum_{j=1}^N S_{ij} S_{il} \sigma_{jk}^{MC} \sigma_{hl}^{MC}, \quad (16)$$

or, equivalently:

$$D = 2\sigma_{MC} S^\dagger \Sigma^{-1} S \sigma_{MC}. \quad (17)$$

### A. Entropy evaluation

In usual MaxEnt implementations, minimization data are wasted and information about the system is inferred solely from the final probability distribution. Here we show how to recycle the whole minimization procedure to infer the entropy of the system. In fact, computing the entropy directly from the converged probability distribution is a very challenging task. However, entropy can be obtained from an adiabatic integration through the minimization path of the Hamiltonians. The values of the observables during the minimization can be used to obtain a measurement of the entropy of the system without any further Monte Carlo computation.

To compute entropy, it is convenient to define, as done for the effective Hamiltonian, an auxiliary function that is equivalent to the Helmholtz free energy:

$$F = -\ln Z,$$

which can be computed through a thermodynamic integration along the minimization path. Then, Entropy is obtained by inverse Legendre transformation from the auxiliary free energy of the system. Even if the free energy is not well defined (the energy is defined up to a constant), the entropy is.

The free energy at the final value of the minimization is:

$$F(\xi = 1) = F_0 + \int_0^1 \frac{dF}{d\xi} d\xi, \quad (18)$$

where  $\xi$  is a variable that parametrizes the path of the Hamiltonian during the minimization. The  $F_0$  value is the free energy at the starting condition, that is the non-interacting system.

$$F_0 = -M \ln \left( \sum_{j=1}^q e^{-\beta \lambda_j(0)} \right), \quad (19)$$

---


$$S[\lambda_i(\xi)] = M \ln \left( \sum_{j=1}^q e^{-\lambda_j(0)} \right) + \sum_{i=1}^N \left[ \lambda_i(1) \langle x_i \rangle_1 - \int_0^1 d\xi \frac{d\lambda_i}{d\xi}(\xi) \langle x_i \rangle_\xi \right]. \quad (25)$$


---

The only required quantities are the Hamiltonian during the minimization, i.e. the  $\lambda_i(\xi)$ , and the values of the observables  $\langle x_i \rangle_\xi$ , both already computed during the minimization. In addition, if all the configurations generated during the  $\chi^2$  minimization are stored, the importance sampling (IS) can be used to interpolate between different Monte-Carlo points, providing a very good sampling of the integral. IS implementation for the minimization is discussed in Appendix B.

$$F_\xi = -\ln Z_\xi, \quad (20)$$

$$\frac{dF}{d\xi} = \left\langle \frac{dH_\xi}{d\xi} \right\rangle_\xi. \quad (21)$$

The integral can be done parametrizing the Hamiltonian as:

$$H_\xi = \sum_{i=1}^N \lambda_i(\xi) x_i, \quad (22)$$

where  $x_i$  are the observables while  $\lambda_i$  are both the Lagrangian multipliers of the MaxEnt algorithm and the parameters through which the  $\chi^2$  function is minimized. Therefore we get:

$$\frac{dF}{d\xi} = \sum_{i=1}^N \frac{d\lambda_i}{d\xi} \langle x_i \rangle_\xi, \quad (23)$$

so that only the averages of the observables during the minimization are required in order to compute the free energy:

$$F = \langle H \rangle - TS, \quad (24a)$$

$$S = \frac{\langle H \rangle - F}{T}. \quad (24b)$$

Fixing  $T = 1$ , we obtain:

### B. Least maximum entropy principle

Entropy can be defined in the framework of a least principle. The MaxEnt approach finds the probability distribution that maximizes the entropy on the subset where the expected values of the observables  $x_i$  are constrained. The entropy  $S_{ME}$  associated with the MaxEnt probability distribution is greater than the true entropy  $S_{real}$  of the system since the true  $P$  lies in the chosen

subset.

$$S_{real} \leq S_{ME}. \quad (26)$$

Moreover,  $S_{ME}$  decreases whereas new constraints are added due to a contraction of the probability distribution space. In Appendix C we provide a rigorous proof of the fact that a set of constraints that ensures Eq. (26) to become an equality exists. The true entropy of the system is then the least maximum entropy of all possible choices of the constraints.

Just like any variational least energy principle in physics, from Hartree-Fock to *density functional theory* (DFT), the energy (entropy in our case) and its derivatives are the targets of the theory, while the wave functions (probability distributions) are *side-effects*. We want to remark that the error on the entropy due to the limited number of constraints is of second order, while the resulting probability distribution is affected by a first order error.

### III. ECOSYSTEM ANALYSIS

Although the so far introduced method is quite general, we discuss its implication in ecosystems. In particular, we analyze a two dimensional model on a regular 2D lattice of edge  $L$  (number of nodes  $M = L^2$ ), whose sites can either be empty or occupied by a fish or a shark. In the application of the MaxEnt algorithm, we limited the constraints  $x_i$  introduced in Eq. (2) to the numbers of preys and predators and near-neighbor fish-fish, shark-shark and fish-shark couples. The corresponding MaxEnt Hamiltonian describes a three-state Potts model [52].

#### A. Model definition

Along the lines of Dewdney [33] and Mobilia et al. [34], we modeled a minimal ecosystem composed of two species interacting each other as a 2D lattice model. Each site can be occupied either by the environment or a fish or a shark, respectively represented with the integers 0,1,2. At every time step, fishes can move, breed or remain still with probability  $p_f^m$ ,  $p_f^f$  and  $1 - p_f^m - p_f^f$ . Sharks can move ( $p_s^m$ ) or remain still ( $1 - p_s^m$ ). Furthermore, sharks eat fishes whenever they step into a cell occupied by a prey. In this case, sharks can reproduce with probability  $p_s^f$ . If a shark does not eat a fish during its round, it can die with probability  $p_s^d$ . This set of rules defines a Markovian process described by the transition matrix  $\Pi(\vec{\sigma}_i \rightarrow \vec{\sigma}_j)$ . It gives the probability of the system to transit from the  $\vec{\sigma}_i$  to the  $\vec{\sigma}_j$  state, where  $\vec{\sigma}_x$  identifies the values of all sites in the lattice. The probability to find the system in the  $\vec{\sigma}_i$  state at the  $t + 1$  time step is defined by:

$$P(\vec{\sigma}_i, t + 1) = \sum_{\vec{\sigma}_j} \Pi(\vec{\sigma}_j \rightarrow \vec{\sigma}_i) P(\vec{\sigma}_j, t). \quad (27)$$

Studying the time evolution of  $P(\vec{\sigma}, t)$  through Dynamical Monte Carlo simulations (see appendix D) it is possible to assess that the system reaches a steady state distribution:

$$P(\vec{\sigma}_i) = \sum_{\vec{\sigma}_j} \Pi(\vec{\sigma}_j \rightarrow \vec{\sigma}_i) P(\vec{\sigma}_j). \quad (28)$$

Depending on the choice of the parameters, the system that we named EcoLat (*Ecosystem on Lattice*) presents three different states: i) fish saturation due to the extinction of sharks; ii) life extinction, where sharks eat all fishes and then extinguish. iii) Non-Equilibrium Steady-State (NESS), in which fish and shark densities fluctuate around a constant value.

The probability distribution can be defined by extracting configurations from the evolving system after a transient time. Sampling configurations sufficiently distant in time it is possible to introduce an ergodic hypothesis (appendix E), i.e. the so defined probability distribution is equivalent to the one of an infinite ensemble of independent systems. In this framework, the entropy becomes a well-defined quantity.

It is important to notice that such formulation neglects the time-correlations of the evolving configuration, i.e. it disregards the flux of probability distribution that uniquely characterizes the generic non-equilibrium steady-state [53].

#### B. MaxEnt distribution benchmark

The configurations extracted from EcoLat are used to evaluate the constraints of the MaxEnt distribution (the number of fishes, sharks and near neighbor couples). We found a good agreement between EcoLat and MaxEnt distributions (FIG. 1).

In FIG. 1(a-b) two sample configurations are compared. The general aspect of the system is well reproduced by near neighbors MaxEnt, except the shape of the shoals that exhibits some differences. This is reflected by the spatial correlation functions in FIG. 1(c), computed as the Pearson coefficient:

$$f_{ij}(x) = \frac{\langle \sigma_i(X) \sigma_j(X+x) \rangle - \langle \sigma_i(X) \rangle \langle \sigma_j(X+x) \rangle}{\sqrt{(\langle \sigma_i(X)^2 \rangle - \langle \sigma_i(X) \rangle^2)(\langle \sigma_j(X)^2 \rangle - \langle \sigma_j(X) \rangle^2)}} \quad (29)$$

where  $\sigma_i(X)$  is one if the site  $X$  is occupied by the  $i$ -th species; note that  $f_{ij}$  does not depend on  $X$  thanks to the translational symmetry of the system. MaxEnt approximation, although it maintains the qualitative agreement, predicts lower fish-fish spatial correlation at larger distances. This does not affect the cluster size distribution, see FIG. 1(d), that decays with the same slope both in EcoLat and MaxEnt. The reason can be understood by looking at the snapshot of the configuration in FIG. 1(a-b), where fishes create shoals of similar size but having more roundish shapes in EcoLat than in MaxEnt configuration, explaining the higher spatial correlations even

if shoals exhibit the same size distributions. This is a general feature of the system independent on the choice of the phenotypes. It unveils that, in the dynamical steady-state, fishes cooperatively interact beyond near-neighbors, while all other interactions seem operating on near-neighbor sites.

The power-law decay in EcoLat shoal size distribution (FIG. 1*d*) has been already observed [54] and assigned to a self-organized behavior of the system, moreover, it seems to be a general characteristic of several spatial ecology models [55].

The MaxEnt distribution is very close to a critical point. This can be checked by introducing a parameter  $T$  in analogy to the Boltzmann temperature, however, the  $T$  dependence alone is not an evidence of the criticality in the original system [56].

### C. Entropic curves

Thanks to the method introduced in Eq. (25), it is possible to compute the entropy of the model and to shed light on several features of the ecosystem.

In FIG. 2 we report, as a function of the species relevant phenotypes, the entropy per site of the system normalized by its maximal value  $\ln 3$ . The entropy has been measured both through the mean-field Shannon-Fano algorithm (6a) and with the new approach based on the MaxEnt calculation of Eq. (25). The MaxEnt entropy estimation is always lower than the mean-field result, as expected due to the variational nature of the least-entropy-principle. Regions of phenotype values that lead the system to extinction are filled with oblique lines. FIG. 2(*a-b*), showing entropy curves as a function of  $p_f^f$  and  $p_s^m$  respectively, manifest qualitative differences between Shannon-Fano and MaxEnt entropy trends. In particular, while Shannon-Fano predicted entropies reach a plateau whenever  $p_f^f \gtrsim 0.5$  or  $p_s^m \gtrsim 0.7$ , MaxEnt ones display a maximum around those values. The increasing difference between Shannon-Fano and MaxEnt entropy is a clear sign that structural ordering is occurring since MaxEnt entropy is the exact entropy of the Potts-like Hamiltonian that takes into account spatial correlations even beyond near-neighbor ones (FIG. 1*c*).

This feature, particularly visible in FIG. 2(*b*), is related to the formation of waves of predator and preys (see snapshots in FIG. 3*b*).

Furthermore, extrapolation of FIG. 2(*b-c-d*) entropy curves manifests a sharp point in  $p_s^m = 0.4$ ,  $p_f^f = 0.4$  and  $p_s^d = 0.6$ , which are a peculiar sign of a second order phase transition between coexistence and extinction. On the contrary, when  $p_s^m = 0.9$  or  $p_s^d = 0.1$  entropy displays a sudden jump into the extinction phase. This transition is due to a finite size effect [57, 58]: increasing the lattice size the probability of the system to extinguish in a fixed time becomes sharper as a function of phenotypes but the transition threshold drifts to the bond value  $p_s^m = 0$  in the thermodynamic limit.

### D. Discussion

The measurement of disorder provides a new insight into the ecosystem. It allows us to recognize the second order phase transition near predator extinction threshold, to characterize the self-organized behavior of prey shoals, and to unveil the increase of structural ordering the system acquires improving the predator hunting capability. Here we discuss these findings following the ecosystem behavior while tuning the shark mobility ( $p_s^m$ ) as in FIG. 2(*b*) since it is a particularly explicative parameter of the model. Increasing the shark mobility the system passes from an absorbing state where the lattice is crowded with preys to a phase in which sharks start appearing in small shoals swimming in a sea of fishes. This is a critical point known in literature [32, 35, 36] and it was characterized by its dynamical properties, where predator population decays in time with a power-law and it belongs to the directed percolation universality class. The criticality of this point is reflected in the entropy behavior which manifests a sharp point.

This phase transition, marking the passage between species coexistence and extinction, happens where the entropy reaches zero (sharp points in FIG. 2(*a-b-c*) at  $p_s^m = 0.4$ ,  $p_f^f = 0.4$  and  $p_s^d = 0.6$ ), and can be attained diminishing the shark hunting ability as well as their fertility or increasing their mortality. The zero entropy of this critical point can be explained in a Shannon-Fano framework, in fact, the predominance of preys unbalances the average numbers of sharks and fishes.

Moving away from the aforesaid criticality, fish clusters acquire a power-law distribution [55] well described by the MaxEnt approximation (FIG. 1). Very interestingly, this kind of distribution cannot be simply explained in a Shannon-Fano framework. In fact, if we simulate an independent size model, fixing the densities as the real EcoLat ones, we obtain the cluster size distribution of FIG. 3(*a*) that does not match with the EcoLat one. Moreover, the Fisher exponent of the EcoLat distribution varies in the studied parameter ranges between 1.5 and 3 and does not match with the fixed 2.05 one of the independent-site model at the percolation threshold (ordinary percolation). It is worth to notice that the observed power-law is completely accounted for and described by near-neighbor interactions, as the MaxEnt approach is able to quantitatively reproduce it (FIG. 1*d*). Furthermore, the MaxEnt Hamiltonian is very close to a critical point. Even if this feature alone is not a signature that the real EcoLat is itself close to a criticality [56], the MaxEnt power-law cluster distribution is related to this criticality. Is the power-law distribution a marker of self-organized criticality in the EcoLat model? The excellent accordance with the critical MaxEnt power-law seems to support this hypothesis.

Increasing  $p_s^m$  from the directed percolation critical point we see the disorder growing (first two snapshots of FIG. 3*b*). At first, the system starts getting rid of fish dominance (i.e. it moves away from direct percolation

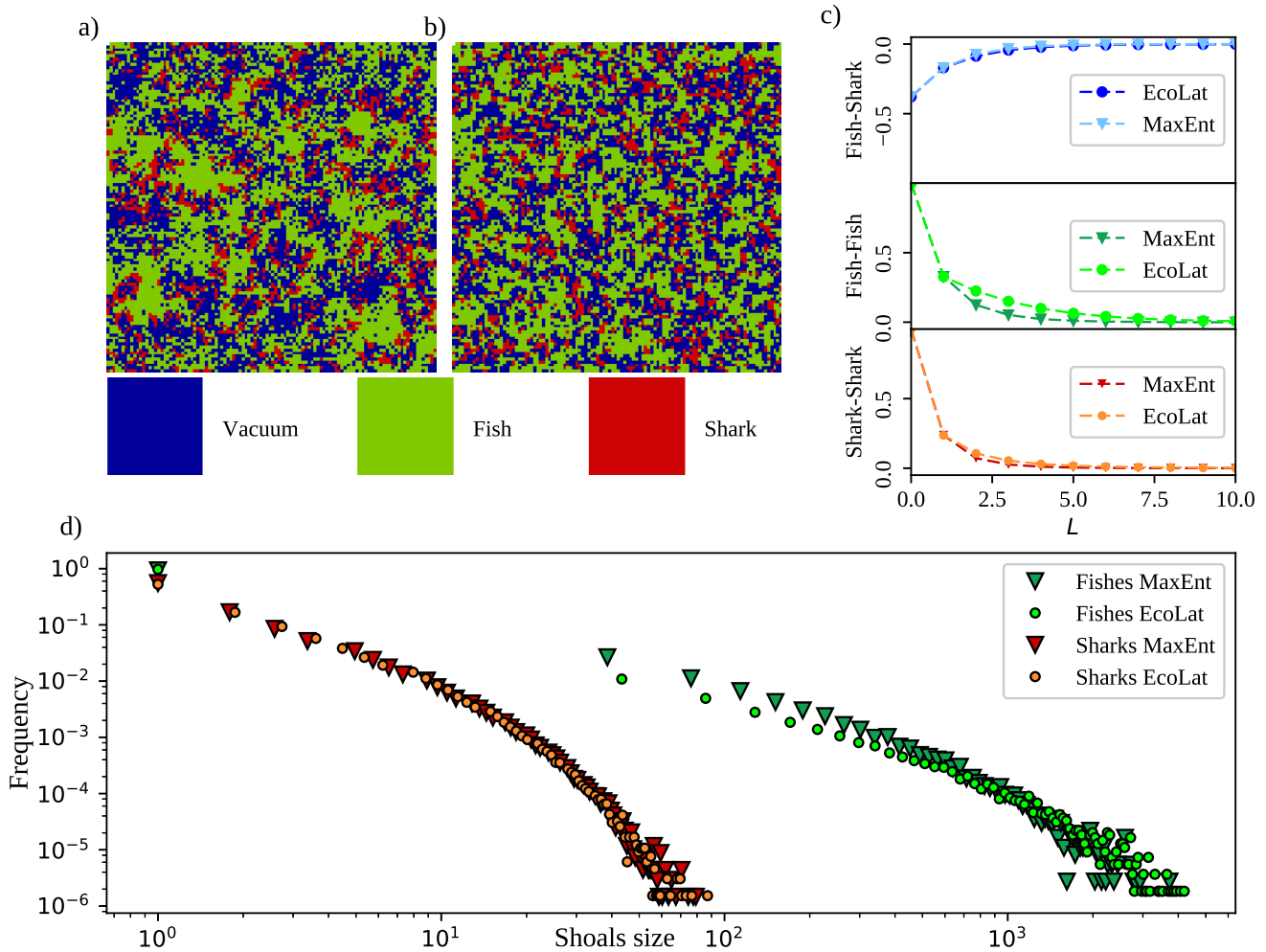


FIG. 1: (Color online) Comparison between the modeled ecosystem (EcoLat) and the Maximum Entropy (MaxEnt) result. **a** Representation of an EcoLat snapshot in the steady-state regime. Fishes are colored in green, sharks in red, while blue represents the environment. Phenotypic parameters are reported in Appendix F. **b** A configuration extracted from the MaxEnt probability distribution obtained by constraining the numbers of fishes, sharks and near neighbor couples. Both simulations ran on a lattice of edge  $L = 110$ . **c** Spatial correlation functions of fish-shark (top), fish-fish (medium) and shark-shark (bottom). **d**. Shoal size distribution of fishes (green shades) and sharks (red shades) computed on EcoLat (circles) and MaxEnt (triangles) configurations. Fishes are power-law distributed, while sharks exhibit an exponential decay.

critical point) simply increasing the number of predators. Both the higher number of sharks and their increased motility make the ecosystem drift toward more disordered configurations (both Shannon-Fano and MaxEnt entropies increase). At a certain point, the interactions between species dominate and the system passes to a regime where it starts regaining order. From FIG. 2(b) and FIG. 3, we see that entropy discriminates these two distinct dynamical behaviours of species at coexistence: the one with a predominance of fishes and sharks grouping in small shoals, and the other where both preys and predators form elaborate shoals, characterized by a spreading wave-like fronts of fishes and sharks [32, 59] with predators surrounding the shoals of preys (FIG. 3b). Very interestingly, this crossover is clearly characterized

by a decreasing MaxEnt entropy with respect to a constant Shannon-Fano one (FIG. 2b), remarking the structuring of the system and the impossibility of grasping this behavior just considering the mean-field approximation. The progressive re-achievement of order can be visualized by looking at the last two EcoLat snapshots in the steady-state regime (FIG. 3b). Notably, this new structural order is very different from the mean-field order close to the shark extinction threshold (last vs first snapshots of FIG. 3b). The structural order can be measured as the difference between Shannon-Fano and MaxEnt entropy. In fact, Shannon-Fano order is a mean-field quantity that does not depend on the disposition of species in the lattice, while MaxEnt entropy considers the order resulting from all possible correlations reproduced by a three-state

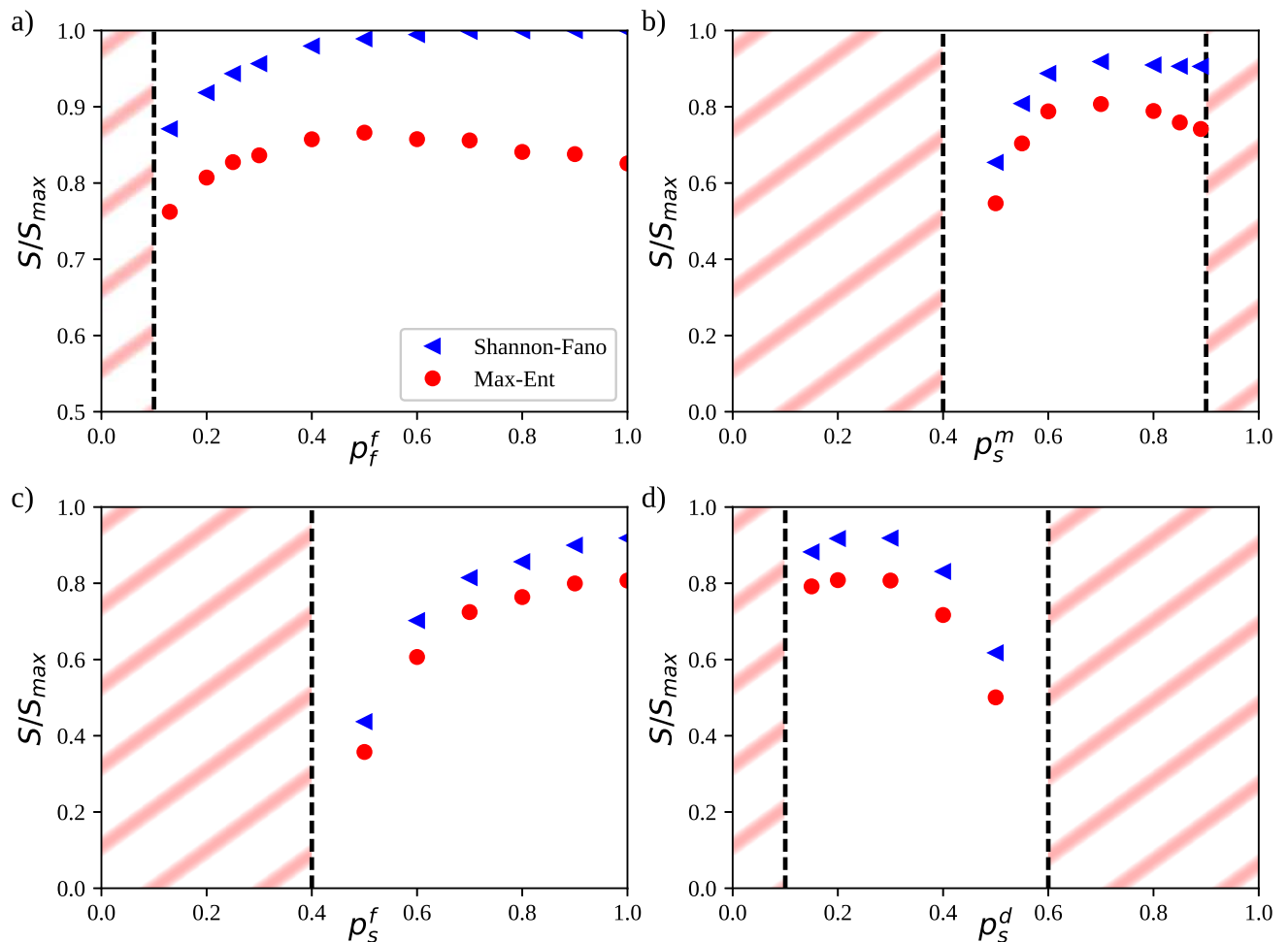


FIG. 2: (Color online) Entropy per site as a function of species phenotypes. Blue triangles indicate the Shannon-Fano entropy (6a) while red circles the MaxEnt entropy (25). The ranges of parameters that lead species to extinction are underlined by oblique lines. **a)** Entropy vs fish breeding probability. A qualitative difference in the entropy behaviors appear when  $p_f^f > 0.5$ ; MaxEnt entropy starts decreasing while Shannon-Fano one saturates to the maximum value. **b)** Entropy vs shark mobility. Also in this case a similar difference in behaviors manifests in the region  $0.7 < p_s^m < 0.9$ . These differences outline that structural ordering is occurring in the system. **c)** Entropy vs shark filiation. **d)** Entropy vs shark mortality. In these two cases, the Shannon-Fano approximation grasps qualitatively well the entropy trends, although the numerical values are overestimated.

Potts model. An analogy with the Ising model (where the MaxEnt algorithm is exact) gives a clearer picture: in the overcritical region,  $T > T_c$  and no external magnetic field, the Shannon-Fano entropy is always at its maximum value since there is an equal number of spin up and spin down. However, the true entropy decreases as  $T \rightarrow T_c$  since ordered spin domains appear.

Finally, another transition between coexistence and extinction is reached by further increasing the shark mobility (as well as decreasing the fish fertility and shark mortality). Contrariwise to the first critical point, the entropy does not continuously go to zero in correspondence of the phase transition, but abruptly jumps to zero (FIG. 2). This is a finite-size effect [57, 58] that disappears when  $L \rightarrow \infty$ . It is worth to notice that, at fixed  $L$ ,

it is possible to continuously tune the phenotype in order to get a steady-state metastable phase even in the extinction region that lives until a sufficiently large stochastic fluctuation causes a brutal extinction. This is very worrying; in fact, it is difficult to predict since no precursors are present and can bring to an ecological catastrophe.

#### IV. CONCLUSIONS

Entropy measurements in complex systems have always been challenging. MaxEnt is a powerful tool to obtain an estimation of the probability distribution of the system from simulations or experimental data. Until now, the information provided by the intermediate



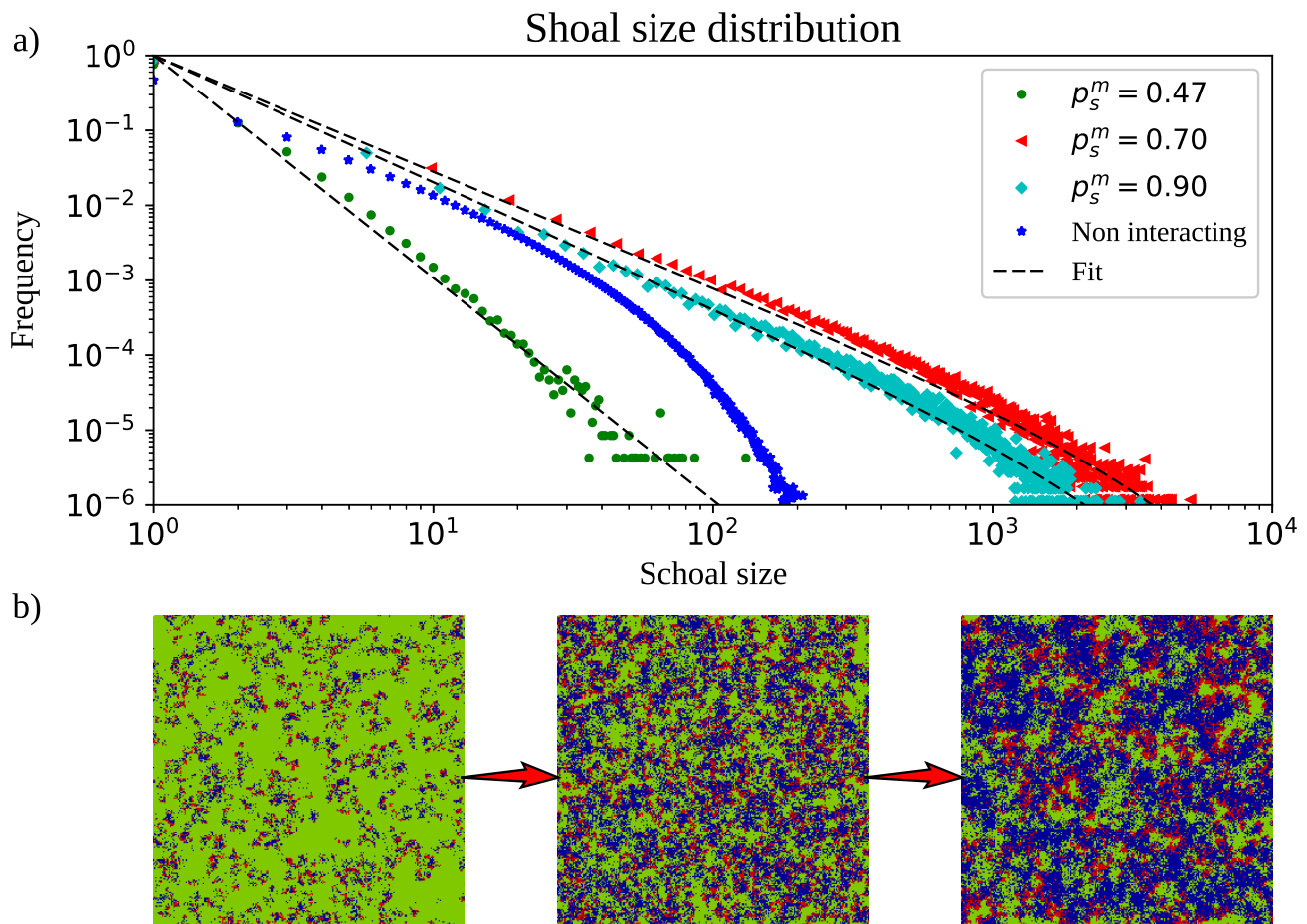


FIG. 3: (Color online) **a** Distributions of prey shoal sizes for three different values of predator mobility (all parameters are reported in Appendix F). Distributions for  $p_s^m = 0.47, 0.70, 0.90$  are shown in green dots, red triangles and cyan diamonds respectively. Blue stars represent the distribution of the independent-site model (Noninteracting) with the fish density fixed to match the EcoLat one with  $p_s^m = 0.7$ . The EcoLat distributions have been fitted with a function  $x^{-\gamma} \exp(x/\xi)$ . The lower mobility case has  $\xi = \infty$  and  $\gamma = 2.97 \pm 0.04$ , medium mobility has  $\xi = 3450 \pm 220$  and  $\gamma = 1.55 \pm 0.01$ , while high shark motility gives a fish shoal distribution with  $\xi = 2440 \pm 180$  and  $\gamma = 1.69 \pm 0.01$ . **b** Snapshots taken from the EcoLat steady state distribution while tuning the shark mobility  $p_s^m$  from 0.47 (left) to 0.90 (right). Fishes are depicted in green, sharks in red, empty sites in blue.

steps of the MaxEnt solution was wasted. We introduce a way to recycle it in order to directly evaluate the entropy of the system without any further time-consuming computation (Eq. 25). Thanks to the MaxEnt nature of the probability distribution, a variational principle for entropy evaluation of the real system can be formulated, which ensures that the obtained entropy is always greater or equal to its true value. Moreover, Eq. (25) is quite general, allowing to compute entropy where it is possible to formulate a MaxEnt algorithm.

Among many possible applications, the knowledge of entropy in ecological systems plays a pivotal role describing the complexity due to the phenotype variability. In the studied prey-predator ecosystem, it sheds new light on the self-organizing behavior of preys. The di-

rect near-neighbor correlations used in our MaxEnt approach are found to be the fundamental ingredient in this self-organized behavior: The MaxEnt Hamiltonian quantitatively reproduces the scale-free behavior of the prey shoals size, where the simpler mean-field approach fails. Furthermore, entropy allows the measurement of structural ordering, that is found to be a key ingredient in characterizing the crossover between two different coexistence behaviors, one where predators form localized patches (dominated by mean-field disorder) and another where predators chase preys in spreading prey-predator fronts (dominated by structural order).

As a matter of fact, the entropy curves reported in FIG. 2 are a powerful tool to investigate the system from quite different perspectives. This new tool will enable the

study of entropic-driven phenomena, like entropic forces, already found to be of great importance in many biological systems as flocks of birds [7].

Furthermore, the general nature of the method encourages its application in many other systems of interest.

### Acknowledgments

The authors would like to thank Francesca Tria, Vito D.P. Servedio and Vittorio Loreto for useful insights, Andrea De Martino and Francesco Mauri for helpful discussions.

### Appendix A: Mean-field MaxEnt

Here we derive Eq. (5). In the mean-field approximation, only one body observables  $\{x_i\}_{i=1}^q$  are constrained, e.g.  $\langle x_i \rangle$  is the average number of nodes in the  $i$ -th state. Now, Eq. (4) describes a non-interacting effective Hamiltonian.

$$\langle x_i \rangle = \frac{1}{Z} \sum_{\sigma_1 \dots \sigma_M} \left( \sum_{k=1}^M \delta_{\sigma_k, i} \right) \exp \left( - \sum_{h=1}^q \lambda_h \sum_{k=1}^M \delta_{\sigma_k, h} \right), \quad (\text{A1})$$

where  $Z$  is the normalization of the probability distribution and we identified the configuration  $\vec{\sigma}$  with its site values:

$$\vec{\sigma} = \begin{pmatrix} \sigma_1 \\ \sigma_2 \\ \vdots \\ \sigma_M \end{pmatrix}. \quad (\text{A2})$$

The  $\left( \sum_{k=1}^M \delta_{\sigma_k, i} \right)$  is the application of the  $x_i$  observable on the  $\vec{\sigma}$  state. Since  $x_i$  does not depend on the particular site  $k$  we have:

$$\langle x_i \rangle = M \frac{e^{-\lambda_i}}{\sum_{h=1}^q e^{-\lambda_h}}. \quad (\text{A3})$$

Eq. (A3) defines a complete set of linear equations. They are dependent since we have the constraint:

$$\sum_{i=1}^q \langle x_i \rangle = M \quad (\text{A4})$$

It is straightforward to show that the most general solution of the system is given by:

$$\lambda_i = -\log \left( \frac{\langle x_i \rangle}{M} \right) + C \quad (\text{A5})$$

where  $C$  is an arbitrary constant that does not affect any physical quantity. For sake of simplicity, in Eq. (5) we set  $C = 0$ .

### Appendix B: Importance sampling

The minimization of Eq. (8) is computationally expensive. In each step, the expected values of the observables for the trial set of  $\lambda_i$  parameters must be computed through a Monte Carlo-Metropolis integration. A natural extension of the Metropolis algorithm consists of re-weighting the extracted configurations at each step. This method takes the name of Importance Sampling (IS) and it has been widely applied in many physical applications [60, 61]. It was introduced in MaxEnt by Broderick et al. [62].

The average of an observable with an Hamiltonian  $H'$  can be computed using a set uniform distributed configurations  $\{c\}_{i=1}^{N_c}$  as follows:

$$\langle A \rangle_{H'} = \sum_{i=1}^{N_c} \left( A(c_i) \frac{P_{H'}(c_i)}{P_H(c_i)} \right) P_H(c_i) = \langle A \frac{P_{H'}}{P_H} \rangle_H. \quad (\text{B1})$$

This average can be computed using Monte Carlo integration on a set of Metropolis extracted configurations  $\{c'\}_{i=1}^{N_c}$  with the  $H$  Hamiltonian:

$$\langle A \rangle_{H'} \approx \frac{1}{Z(N_c)} \sum_{i=1}^{N_c} A(c'_i) e^{-\beta[H'(c'_i) - H(c'_i)]}, \quad (\text{B2a})$$

$$Z(N_c) = \sum_{i=1}^{N_c} e^{-\beta[H'(c'_i) - H(c'_i)]}. \quad (\text{B2b})$$

Handling with large lattices, energy differences can be considerable, and the exponential term may give rise to numerical instabilities. To correct these instabilities a constant factor  $a$  can be added to both exponential terms, equal to the maximum energy difference of all extracted configurations.

Estimating the goodness of IS in MaxEnt implementation can be difficult. In fact, we lack the *a priori* knowledge of the partition function of the original probability distribution. In order to upstage, the problem we implemented a new statistical evaluator for the MaxEnt algorithm and in general for IS Metropolis implementation. At each step the total extracted configurations are divided into two random groups and the normalization factors are compared:

$$\eta = \left| \frac{Z'(N_c/2)}{Z''(N_c/2)} - 1 \right|. \quad (\text{B3})$$

If  $\eta$  exceeds a critical value  $\eta_c$ , new configurations are extracted from the Metropolis algorithm. FIG. 4 shows the performance of IS vs the  $\eta_c$  parameter. For  $\eta_c \ll 1$ , Eq. (B3) is symmetric with respect to  $Z'$  and  $Z''$ . For higher values of  $\eta_c$  the symmetry is recovered by random shuffling the configurations at each step.

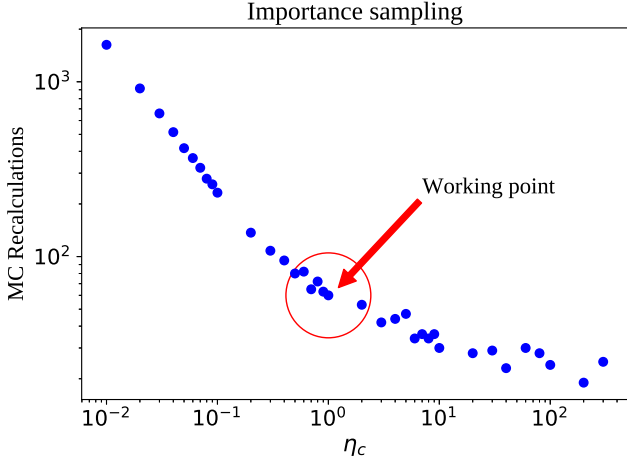


FIG. 4: (Color online) Number of Monte Carlo simulations to reach convergence as a function of the  $\eta_c$  parameter (B3). The optimal working point lies in the marked region.

### Appendix C: Proof of the least maximum entropy principle

By definition, the MaxEnt entropy is always greater than the true entropy:

$$S_{real} \leq S_{ME}[\{\hat{x}_i\}] \quad (C1)$$

where  $S_{real}$  is the real entropy of the system, while  $S_{ME}[\{\hat{x}_i\}]$  is the maximum entropy of all possible probability distributions that fix the set of  $\hat{x}_i$  observables.

To prove the least maximum entropy principle, a set of observables  $\hat{x}_i$  must exist so that Eq. (C1) is an equality. In any finite size system, where configurations can be represented with a finite dimension vector, this is trivial, since it is possible to choose a set of observables  $\hat{y}_i$  defined as:

$$\hat{y}_i(\vec{\sigma}) = \delta(\vec{\sigma}, \vec{\sigma}_i), \quad (C2)$$

where  $\vec{\sigma}$  is the configuration on which the observables act,  $\vec{\sigma}_i$  is a particular configuration associated with the observable  $\hat{y}_i$  and  $\delta$  is the Kronecker symbol.

If two probability distributions are different, then a configuration  $\vec{\sigma}_i$  must exist so that their probabilities differ:

$$p_1(\vec{\sigma}_i) \neq p_2(\vec{\sigma}_i). \quad (C3)$$

The two distributions give two distinct expected values for the corresponding  $\hat{y}_i$  observable:

$$\langle y_i \rangle_{p_1} = \sum_j p_1(\vec{\sigma}_j) \delta(\vec{\sigma}_j, \vec{\sigma}_i) = p_1(\vec{\sigma}_i) \neq p_2(\vec{\sigma}_i) = \langle y_i \rangle_{p_2}. \quad (C4)$$

The complete set of  $\hat{y}_i$  fixes the probability distribution, so that

$$S_{real} = S_{ME}[\{\hat{y}_i\}]. \quad (C5)$$

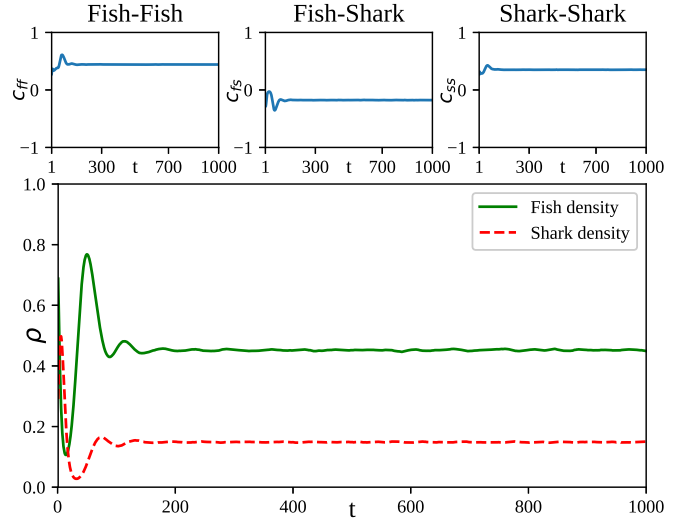


FIG. 5: Time evolution of the mean fish and shark densities and near-neighbour Pearson correlation coefficients computed on an ensemble composed by 100 replicas of the system. The simulation is prepared in an initial uniform distribution fixing the densities of preys and predators to 4/5 and 1/5 respectively.

Indeed, single-site density and couple density can be written as linear combination of the complete set of  $\hat{y}_i$  observables. Therefore, the introduction of more independent constraints assures the convergence of the MaxEnt entropy toward the real entropy.

### Appendix D: Dynamical Monte Carlo simulations of the EcoLat model

Dynamical Monte Carlo allows us to simulate the EcoLat master equation (Eq. 27). Since the number of possible states is huge ( $3^M$ ) it is impossible to numerically evolve the probability distribution. However, a stochastic solution of Eq. (27) is still possible:  $N$  replicas of the system, extracted according to an initial distribution  $P(\vec{\sigma}, 0)$ , can be evolved according to the transition matrix  $\Pi$ . The obtained time-dependent ensemble can be used to compute the averages of any observable as a function of time.

The EcoLat model reaches the asymptotic steady-state distribution described by Eq. (28). FIG. 5 shows the time dependence of the mean density of preys and predators as well as the near-neighbor correlation coefficients (Eq. 29).

Note that, although the time evolution of the single system continues to oscillate in the steady-state, the correlation time is finite. This assures that, after a transient time, all the  $N$  simulations are independent and distributed according to the  $P(\vec{\sigma})$  (Eq. 28).

## Appendix E: Ergodic hypothesis

Here we discuss the stability of the steady-state distribution that depends on the ergodicity of the system [63]. Generally speaking, a system is ergodic if it can move between any couple of points in the phase-space in a finite number of steps [64]. EcoLat does not satisfy this requirement, in fact, two traps are present in the phase-space: if the system gets a configuration without preys or predators, it always evolves toward an absorbing state. However, in simulations, once the system has reached the non-absorbing steady-state (FIG. 5), it remains there during all the simulation time. So, we can postulate a weak ergodic hypothesis, where we imagine to restrict the feasible phase-space excluding the absorbing traps. This is equivalent to neglecting the elements of the  $\Pi$  transition matrix that lead the system into the absorbing traps. Such an approximation makes sense if the lifetime  $\tau$  of

the meta-stable equilibrium is much larger than the typical time scales of the system. All the Dynamical Monte Carlo simulations computed in FIG. 2 have  $\tau \gg t_{max}$ , where  $t_{max}$  is the maximum simulation time ( $10^6$ ).

## Appendix F: Simulation details

Phenotypic parameters for the EcoLat simulation of FIG. 1 are:  $p_f^f = 0.2$ ,  $p_f^m = 0.8$ ,  $p_s^m = 0.7$ ,  $p_s^f = 1$ ,  $p_s^d = 0.3$ . Phenotypic parameters for the EcoLat simulation of FIG. 3 are the same apart for  $p_s^m$  that assumes the values of 0.47, 0.70 and 0.90.

All simulations and computations were carried out using authors handmade C and Python scripts. Python packages NumPy [65], SciPy [66] and Matplotlib [67] were utilized during analysis and figure realization.

- 
- [1] W. Johannsen, *The American Naturalist* **45**, 129 (1911).
- [2] F. B. Churchill, *Journal of the History of Biology* **7**, 5 (1974).
- [3] W. Bialek, *Biophysics: Searching for Principles* (Princeton University Press, 2012).
- [4] S. P. Strong, R. Koberle, R. R. de Ruyter van Steveninck, and W. Bialek, *Physical Review Letters* **80**, 197 (1998).
- [5] I. Nemenman, W. Bialek, and R. de Ruyter van Steveninck, *Physical Review E* **69** (2004).
- [6] W. Bialek, A. Cavagna, I. Giardina, T. Mora, E. Silvestri, M. Viale, and A. M. Walczak, *Proceedings of the National Academy of Sciences* **109**, 4786 (2012).
- [7] M. Castellana, W. Bialek, A. Cavagna, and I. Giardina, *Phys. Rev. E* **93** (2016).
- [8] W. Bialek, I. Nemenman, and N. Tishby, *Neural Computation* **13**, 2409 (2001).
- [9] C. E. Shannon, *Bell System Technical Journal* **30**, 50 (1951).
- [10] J. L. Kelly, *Bell System Technical Journal* **35**, 917 (1956).
- [11] G. C. Philippatos and C. J. Wilson, *Applied Economics* **4**, 209 (1972).
- [12] D. De Martino, F. Capuani, and A. De Martino, *Physical Review E* **96** (2017).
- [13] D. De Martino, F. Capuani, and A. De Martino, *Physical Biology* **13** (2016).
- [14] E. Kussell, *Science* **309**, 2075 (2005).
- [15] M. Weigt, R. A. White, H. Szurmant, J. A. Hoch, and T. Hwa, *Proceedings of the National Academy of Sciences* **106**, 67 (2008).
- [16] A. G. Tansley, *Ecology* **16**, 284 (1935).
- [17] W. C. Allee, *Ecological Monographs* **4**, 541 (1934).
- [18] F. S. Chapin, P. A. Matson, and P. M. Vitousek, *Principles of Terrestrial Ecosystem Ecology* (Springer New York, 2011).
- [19] W. Cooper and D. Blumstein, *Escaping From Predators: An Integrative View of Escape Decisions* (Cambridge University Press, 2015).
- [20] B. A. Belgrad and B. D. Griffen, *Proceedings of the Royal Society B: Biological Sciences* **283** (2016).
- [21] R. S. Olson, A. Hintze, F. C. Dyer, D. B. Knoester, and C. Adami, *Journal of The Royal Society Interface* **10** (2013).
- [22] T. W. Swetnam and J. L. Betancourt, *Journal of Climate* **11**, 3128 (1998).
- [23] P. Kindlmann, H. Yasuda, Y. Kajita, S. Sato, and A. F. G. Dixon, *Frontiers in Ecology and Evolution* **3** (2015).
- [24] N. Bax, *ICES Journal of Marine Science* **55**, 997 (1998).
- [25] A. Lotka, *Proc. Natl. Acad. Sci. U.S* (1920).
- [26] V. Volterra, McGraw-Hill (1931).
- [27] E. E. Holmes, M. A. Lewis, J. E. Banks, and R. R. Veit, *Ecology* **75**, 17 (1994).
- [28] K. Kuto and Y. Yamada, *Journal of Differential Equations* **197**, 315 (2004).
- [29] J. D. Ferreira, C. A. T. Salazar, and P. C. Tabares, *Non-linear Analysis: Real World Applications* **14**, 536 (2013).
- [30] J. E. Satulovsky and T. Tomé, *Physical Review E* **49**, 5073 (1994).
- [31] A. Lipowski, *Physical Review E* **60**, 5179 (1999).
- [32] U. Dobramysl, M. Mobilia, M. Pleimling, and U. C. Täuber, *Journal of Physics A: Mathematical and Theoretical* **51** (2018).
- [33] A. K. Dewdney, *Scientific American* **251**, 14 (1984).
- [34] M. Mobilia, I. T. Georgiev, and U. C. Täuber, *Physical Review E* **73** (2006).
- [35] T. Antal, M. Droz, A. Lipowski, and G. Ódor, *Physical Review E* **64** (2001).
- [36] U. C. Täuber, *Journal of Physics: Conference Series* **319**, 012019 (2011).
- [37] I. Nemenman, F. Shafee, and W. Bialek, in *Advances in neural information processing systems* (2002), pp. 471–478.
- [38] C. E. Shannon, *Bell system technical journal* (1951).
- [39] E. T. Jaynes, *Physical Review* **106**, 620 (1957).
- [40] A. Cavagna, I. Giardina, F. Ginelli, T. Mora, D. Piovani, R. Tavarone, and A. M. Walczak, *Physical Review E* **89** (2014).
- [41] T. Mora, A. M. Walczak, W. Bialek, and C. G. Callan, *Proceedings of the National Academy of Sciences* **107**,

- 5405 (2010).
- [42] E. Schneidman, M. J. Berry, R. Segev, and W. Bialek, *Nature* **440**, 1007 (2006).
- [43] C. E. Shannon, *Bell System Technical Journal* **27**, 379 (1948).
- [44] R. M. Fano, *The transmission of Information* (Cambridge: Massachusetts Institute of Technology, Research Laboratory of Electronics, 1949).
- [45] S. W. Lockless, *Science* **286**, 295 (1999).
- [46] M. Socolich, S. W. Lockless, W. P. Russ, H. Lee, K. H. Gardner, and R. Ranganathan, *Nature* **437**, 512 (2005).
- [47] W. P. Russ, D. M. Lowery, P. Mishra, M. B. Yaffe, and R. Ranganathan, *Nature* **437**, 579 (2005).
- [48] W. Bialek and R. Ranganathan, *ArXiv e-prints* (2007).
- [49] K. Pearson, *Philosophical Magazine Series 6* **2**, 559 (1901).
- [50] H. Hotelling, *Journal of Educational Psychology* **24**, 417 (1933).
- [51] S. G. Nash, *SIAM Journal on Scientific and Statistical Computing* **6**, 599 (1985).
- [52] R. B. Potts and C. Domb, *Mathematical Proceedings of the Cambridge Philosophical Society* **48**, 106 (1952).
- [53] R. K. P. Zia and B. Schmittmann, *Journal of Statistical Mechanics: Theory and Experiment* **2007**, P07012 (2007).
- [54] B. Sutherland and A. Jacobs, *Complex System* **8**, 385 (1994).
- [55] M. Pascual, M. Roy, F. Guichard, and G. Flierl, *Philosophical Transactions of the Royal Society B: Biological Sciences* **357**, 657 (2002).
- [56] I. Mastromatteo and M. Marsili, *Journal of Statistical Mechanics: Theory and Experiment* **2011**, P10012 (2011).
- [57] M. Parker and A. Kamenev, *Phys. Rev. E* **80**, 021129 (2009).
- [58] A. Dobrinevski and E. Frey, *Phys. Rev. E* **85**, 051903 (2012).
- [59] M. Mobilia, I. T. Georgiev, and U. C. Täuber, *Journal of Statistical Physics* **128**, 447 (2007).
- [60] G. Torrie and J. Valleau, *Journal of Computational Physics* **23**, 187 (1977).
- [61] I. Errea, M. Calandra, and F. Mauri, *Physical Review B* **89** (2014).
- [62] T. Broderick, M. Dudik, G. Tkacik, R. E. Schapire, and W. Bialek, *ArXiv e-prints* (2007), 0712.2437.
- [63] K. Huang, *Statistical Mechanics* (Wiley, 2008).
- [64] R. Palmer, *Advances in Physics* **31**, 669 (1982).
- [65] S. van der Walt, S. C. Colbert, and G. Varoquaux, *Computing in Science & Engineering* **13**, 22 (2011).
- [66] E. Jones, T. Oliphant, P. Peterson, et al., *SciPy: Open source scientific tools for Python* (2001).
- [67] J. D. Hunter, *Computing In Science & Engineering* **9**, 90 (2007).